Disclaimer:

Transportation Infrastructure Precast Innovation Center (TRANS-IPIC)

University Transportation Center (UTC)

Data-Driven Smart Composite Reinforcement for Precast Concrete
PU-23-RP-05

FINAL REPORT

Submitted by:
Chengcheng Tao (PI), tao133@purdue.edu
Shanyue Guan (Co-PI), guansy@purdue.edu
School of Construction Management Technology
Purdue University

Collaborators / Partners:
Heidelberg Materials, North Dakota State University

Submitted to:
TRANS-IPIC UTC
University of Illinois Urbana-Champaign
Urbana, IL

Executive Summary (1-page max):

Composite reinforcement has been increasingly applied in the precast concrete structure components because of its high strength, lightweight, high fracture toughness, long-term corrosion, and crack resistance. The behavior of composite reinforcement plays an important role in the precast concrete infrastructure. It is important to monitor the material system and provide real-time situational awareness under different scenarios. Physical testing with trial-and-error approaches on composite reinforced PC components require substantial time, labor, and material resources to monitor the structural and materials conditions and detect failure or anomalies under service.

This study aims to develop a smart composite reinforcement in precast concrete for real-time health condition monitoring using embedded sensors on the composite. The monitoring system can provide the health condition and risk information of the composite reinforcement and investigate the load transfer effectiveness between layers of the reinforcement and the precast concrete. The self-sensed composite reinforcement experimental data will be paired with computational models of composite-concrete system and data-driven machine learning algorithms to predict the risk of the composite reinforcement for a better reinforced precast concrete system. The research integrates smart sensor technology, computational mechanics of materials, and data-driven machine learning algorithms to detect the structural and materials failure and anomaly mechanism and predict the associated risk in a wide range of applications. Three consecutive tasks are as follows:

<u>Task 1. Development and testing of embedded smart sensors for self-sensing composite reinforcement in precast concrete.</u> This task focuses on the smart composite reinforcement development and experimental testing of the smart composite reinforcement in PC. The sensor data and image data from the experiment will be used to validate numerical models in Task 2 and generate database of composite reinforced-concrete system for AI-based condition assessment model in Task 3.

<u>Task 2. Multi-scale multi-physics modeling with finite element analysis for the composite reinforcement mechanical and bonding performance.</u> The task focuses on the development of three-dimensional (3D) finite element analysis models to simulate the mechanical and bonding performance of composite reinforcement and precast concrete. Multiple influencing factors will be considered including type of composite reinforcement, type of concrete materials, and geometry of the structure. The numerical analysis results will be compared and validated by the experimental data in Task 1. As the complement of the sensor data in Task 1, the numerical data will be integrated with sensor data and image data in Task 1 to establish a comprehensive physics-informed database for training AI algorithms in Task 3.

<u>Task 3. AI-Driven Condition Assessment for Composite Reinforced Concrete.</u> This task focuses on the machine learning-based condition assessment and risk analysis using sensor data, image data, and numerical model data from Tasks 1 and 2 to assess and predict the condition and risk level of composite reinforced concrete system.

In addition to the research tasks, the research team also conducted educational and industrial outreach activities including the smart reinforced concrete beam testing day, K-12 education video development, and site visit to concrete materials labs and plants.

Table of Contents

1. Statement of problem 5

2. Research Plan / Tasks 5

2.1 Task 1: Development and testing of embedded smart sensors for self-sensing composite reinforcement in precast concrete 5

2.1.1 Experiment Setup 5

2.1.2 Results from Smart Sensors 8

2.2 Task 2: Multi-scale multi-physics modeling with finite element analysis for the composite reinforcement mechanical and bonding performance 9

2.2.1 Numerical validation 10

2.2.2 Flexural Test Analysis 11

2.2.3 Pullout Test Analysis 12

2.3 Task 3: AI-Driven condition assessment for composite reinforced concrete 13

2.3.1 Condition assessment by DAMAGET prediction 13

2.3.2 Condition Prediction from Images 15

3. Educational outreach activities 16

4. Workforce development activities 17

5. Technology transfer actions 17

6. Papers that include TRANS-IPIC UTC in the acknowledgments section 17

7. Presentations and posters of TRANS-IPIC funded research 17

8. Any other events or activities that highlights the work of TRANS-IPIC research that occurred at your university 18

9. Any mentions/references to TRANS-IPIC in the news or interviews from your research 18

10. References associated with this research project 18

TRANS-IPIC Final Report:

1. Statement of problem

Composite reinforcement has been increasingly applied in the precast concrete (PC) area [1], because of its high strength, lightweight, high fracture toughness, long-term corrosion, and crack resistance. The behavior of composite reinforcement plays an important role in the precast concrete infrastructure. It is important to monitor the material system and provide real-time situational awareness under different scenarios. Physical testing with trial-and-error approaches on composite reinforced PC components require substantial time, labor, and material resources to monitor the structural and materials conditions and detect failure or anomalies under service. There is a lack of an efficient and precise way to monitor and predict the risk of the composite reinforcement for PC components.

The proposed research aims to develop a smart composite reinforcement in precast concrete for real-time health condition monitoring using embedded sensors on the composite. The monitoring system can provide the health condition and risk information of the composite reinforcement and investigate the load transfer effectiveness between layers of the reinforcement and the precast concrete. The self-sensed composite reinforcement experimental data will be paired with computational models of composite-concrete system and data-driven machine learning algorithms to predict the risk of the composite reinforcement for a better reinforced precast concrete system. The research will integrate smart sensor technology, computational mechanics of materials, and data-driven machine learning algorithms to detect the structural and materials failure and anomaly mechanism, and predict the associated risk in a wide range of applications.

2. Research Plan / Tasks

2.1 Task 1: Development and testing of embedded smart sensors for self-sensing composite reinforcement in precast concrete

2.1.1 Experiment Setup

Figure 1 shows the schematic of the testbed for smart composite reinforcement in concrete beam. The composite reinforced concrete beam is subjected to testing using the Forney FHS-400-VFD automatic compression test machine. The span length is set to be 18 in, in accordance with the specified requirements of the ASTMC293 standard. The top anvil is positioned at the center, and two bottom rigid supports are placed 1 in from each edge. To develop smart composite reinforcement, we embed LUNA high-definition fiber optic strain sensors and Vishay micro-measurement strain gauges in this task. The fiber optic sensors have the advantages of being small in size (125 μm in diameter without additional coating), high flexibility (allowing them to wrap around reinforcement), long sensing range (up to 2 km per optic fiber), water-resistance, and affordable cost. Fiber optic sensors provide real-time strain monitoring along the entire length of the fiber. In this study, we embed the fiber optic sensor along the bottom of the composite rebars, with two strain gauges positioned at the ends and the midspan of the rebar, next to the fiber optic sensors. We apply Vishay micro-measurement strain gauges on the rebar at various points next to the fiber optic sensor for comparison and validation between two types of smart sensors. In addition to the embedded fiber optic sensors and strain gauges for the composite rebar, as well as linear strain gauges for the concrete. We also equip four image data collection devices, including cell phones, digital image correlation (DIC) cameras, GoPro, and drones. Two phones (iPhone 15 and iPhone 15 ProMax) are placed at the sides to capture deformations of the RC beam. A GoPro camera is attached at the side edge of the beam to observe the propagation of the bending crack. The Intel RealSense digital image correlation cameras face the front and back surfaces of the beam after failure. The DJI drone flies in the diagonally upward direction, filming the experiment and observing the top of beam.

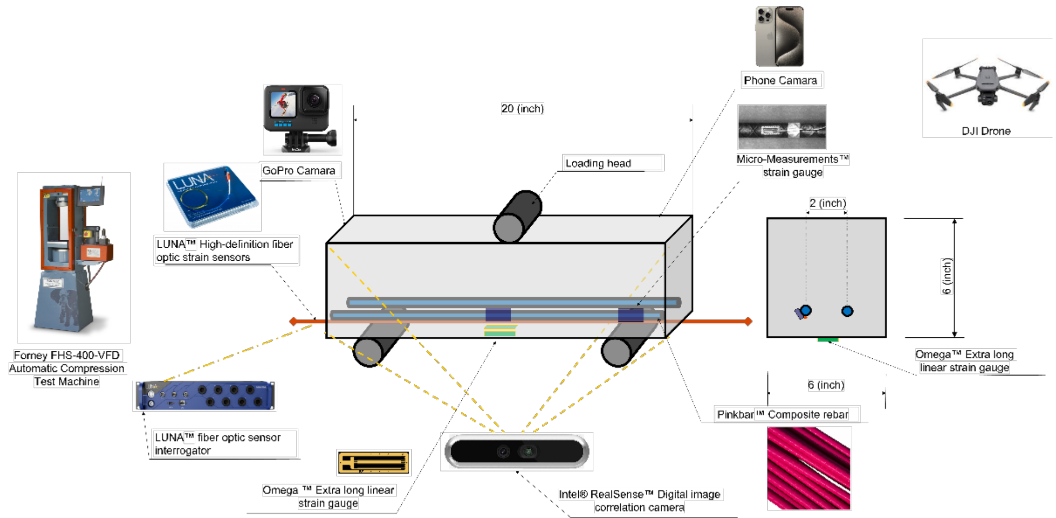

Figure 1. The schematic of the experimental setup of the smart composite reinforced concrete system.

Since the fiber optic sensor is very fragile and vulnerable, we create a groove on the composite rebar to embed the fiber optic sensor, using the method suggested by Bado et al. [2]. Figure 2(a) shows the groove on the rebar for fiber optic sensor embedment. Given the slim and delicate property of fiber optic sensors, we protect them with the coating of 3M DP460 two-component epoxy, which also serves as a glue to ensure strong bonding between the sensor and rebar, as depicted in Figure 2(b). A thin silica tube is used to provide extra protection near the rebar ends, mitigating the risk of fiber fracture. The same two-component epoxy is employed to attach two strain gauges at the midspan and end of the rebar next to the fiber optic sensor. Due to the high curvature of the rebar surface, as shown in Figure 2(b), a vacuum vise and rubber pad are used to secure the strain gauge firmly to the rebar. Once the epoxy has fully cured, the strain gauge functionality is tested using a micro-measurement data analyzer to verify that all gauges are operating correctly, as shown in Figure 2(c).

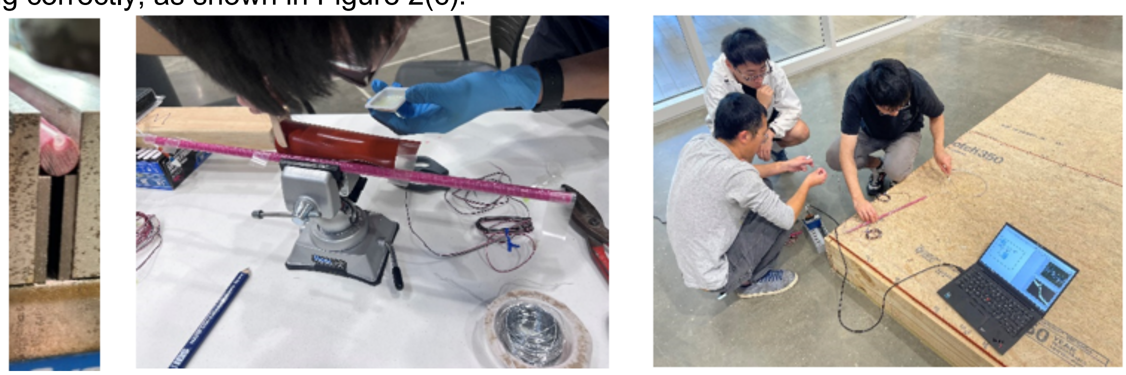

(a) (b) (c)

Figure 2. Smart sensor embedment into composite reinforcement: (a) creating a groove on the composite rebar for fiber optic sensor installation and protection; (b) applying two-component epoxy on fiber optic sensor; (c) testing the workability of rebar strain gauge.

For the development of a smart sensor-based testbed for composite reinforcement in concrete, we conduct a three-point flexural test for a smart composite reinforced concrete beam, following the ASTM C293 and ACI 440.1R standards to evaluate the performance of sensors. The RC beam is configured with cross-sectional dimensions of 6 x 6 inches and a length of 20 inches. Two #3 rebars are positioned with a bottom cover depth of 1 inch, evenly spaced on the rebar chairs. A silica tube is utilized to protect the fiber optic sensor within the concrete, and a PVC tube for the protection in the external parts. We select commercially available ready-mix concrete with a compressive strength of 5000 psi and pour it into a stainless-steel mold for curing. In addition to the fiber optic sensor and strain gauge on rebar, this study incorporates the Omega extra-long linear strain gauge for concrete. We select two measurement locations: one at the bottom center of the beam to capture tensile strain data during the experiment, and another at the corresponding position of the rebars on the front surface, which will provide strain measurements close to the rebars. During the flexural test, we use the fiber optic sensor interrogator and National Instrument data acquisition system (*NI-9235*) with LabView software to collect and monitor strain data along the rebars from fiber optic sensors and strain gauges in real-time, as shown in Figure 3(a). The distributed fiber optic sensors use the principle of light scatterings to measure strain distributions along with the composite reinforcement. The backscattering is an intrinsic property of optical media and is caused by the natural impurities and imperfections in the optical fiber core when a short laser pulse is beamed from one end and propagates along with the fiber. The interrogator can capture the changes in light properties and convert them to strain data. Due to the design of the Forney compression test machine, the middle section of the beam is obstructed. Consequently, Figure 3(b) displays the grid lines drawn on the beam surface to assist with cameras positioning and alignment, facilitating image preprocessing. After completing the grid lines, Figure 3(c) shows the composite reinforced concrete beam being moved to the Forney compression test machine. We also manually check the positions of the beam and the top anvil to ensure compliance with the standard, placing an additional leather compression shim between the top anvil and the beam top surface to eliminate any gap. In addition to the smart sensors, we utilize four types of cameras for this experiment: smart phones, digital image correlation cameras, drone and GoPro. Figure 3(d) exhibits a GoPro installed on the edge of beam for recording the entire experiment. Another two cables are connected to the strain gauge interrogator (*NI-9235*) for collecting and transmitting the data from strain gauges. Figure 3(e) shows the placement of a DIC camera at the front, together with two cellphone cameras on the sides. The cables are reorganized carefully to avoid shear rupture of the delicate fiber optic sensors. Figure 3(f) shows the final crack pattern on the beam, with a thin bending crack detected at the midspan and a wide shear crack near the bottom support.

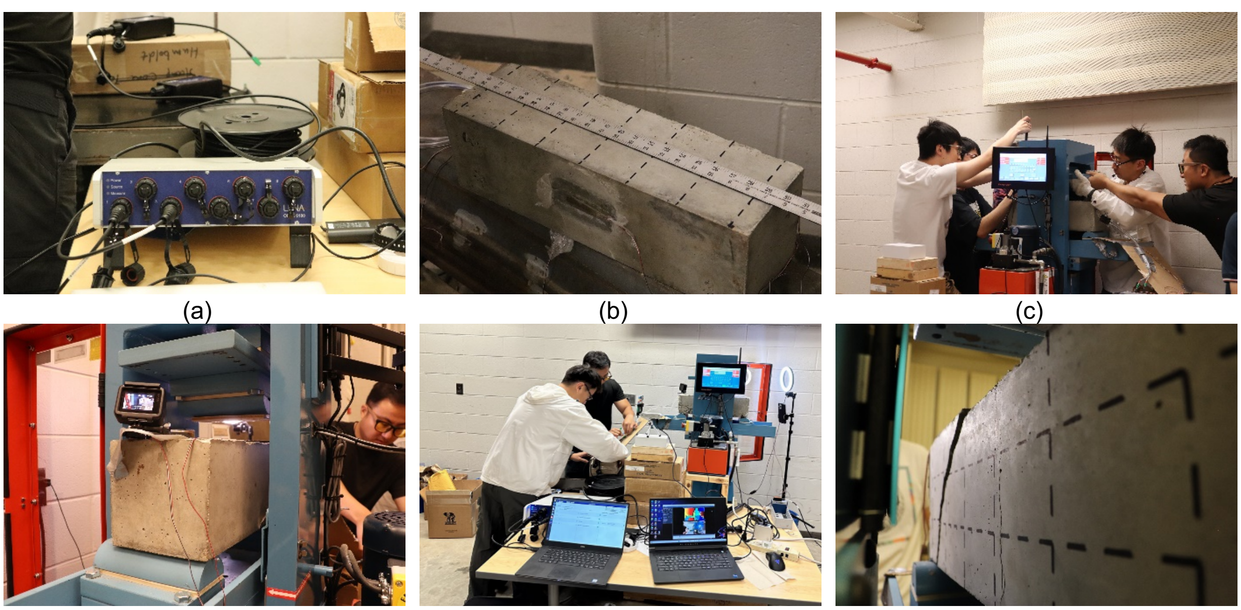

(a) (b) (c)
(d) (e) (f)

Figure 3. Three-point flexural testbed for composite reinforced concrete beam: (a) fiber optic sensor interrogator; (b) grid lines for image preprocessing; (c) transport test sample to test machine; (d) GoPro camara for video recording; (e) sensor and image data collection; (f) final crack propagation pattern.

2.1.2 Results from Smart Sensors

We create two sample beams for the test, Beam 1 is equipped with four strain gauges positioned at the midspan and ends of the rebars, together with two embedded fiber optic sensors along the rebars. Beam 2 also features two fiber optic sensors embedded along the rebars, and two rebar strain gauges at the midspans. For the data collected from the fiber optic sensors, only a portion of the fiber optic sensor data reflect the strain of the composite rebars. Thus, it is essential to determine the appropriate range of data first. As shown in Figure 4, the strain data from the first 0.8 m remains stable, indicating that only the data points after 0.8 m are useful, as highlighted in the red frame. Consequently, we consider the strain data from 0.8 m to 1.25 m as effective strain data for composite rebars, used for further analysis.

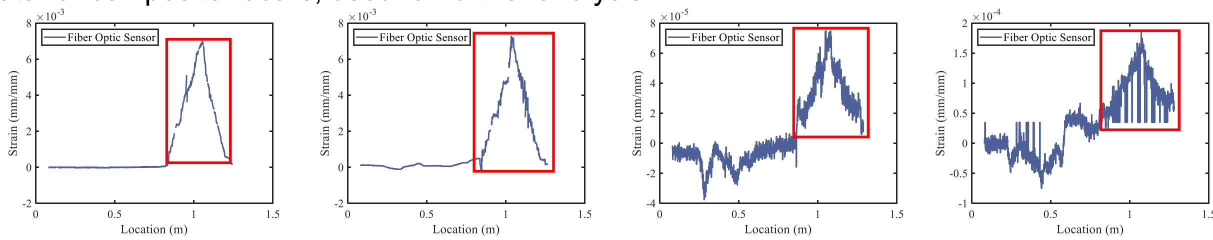

(a) (b) (c) (d)

Figure 4. Raw data from fiber optic sensors: (a) Composite rebar 1 in Beam 1; (b) Composite rebar 2 in Beam 1; (c) Composite rebar 1 in Beam 2; (d) Composite rebar 2 in Beam 2.

We compare the strain gauge results of composite rebars at the midspan and both ends. Since the sensors usually work at relatively high frequencies to capture more data points within a given time, facilitating real-time monitoring, this high frequency can increase noise sensitivity and degrade data quality. To address this, we apply a Butterworth low-pass filter to smooth the signal data and attenuate high-frequency noise, ensuring a gradual transition but keep the important turning points. The sampling rate of the strain gauge is 100 Hz, hence the cutoff frequency is set to be 0.05 Hz. As the two composite rebars are symmetrically placed at the bottom of the composite reinforced concrete beam, the sensors on both rebars should yield similar results. Figure 5(a) displays a plot of the filtered strain gauge results of composite rebars at the midspan. The results from the two rebars are greatly matched, reflecting the bending cracks at 300 s and the shear crack at 620 s. Figure 5(b) – (d) presents the plots that split the entire experiment into three phases: from the beginning to the first crack, from the first crack to the second crack, and from the second crack to the end. The results confirm that the strain gauges function effectively, capturing the occurrence of cracks simultaneously.

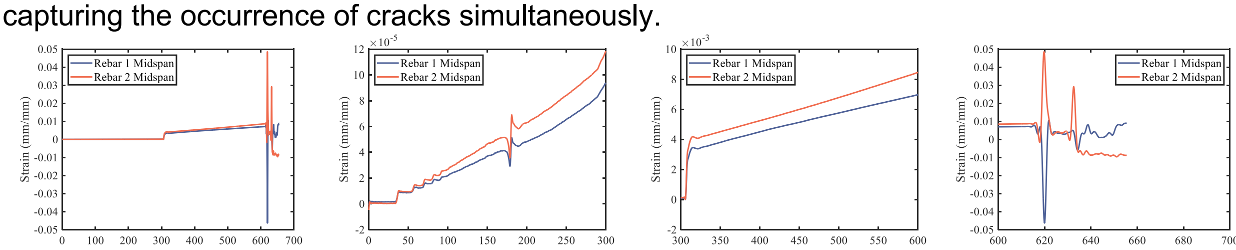

(a) (b) (c) (d)

Figure 5. Strain gauge results of composite rebars at the midspan. (a) Entire experiment time; (b) From the beginning to the time of first crack; (c) From the time of the first crack to the second crack; (d) From the time of the second crack to the end.

Additionally, we conduct a tensile test on the composite reinforcement solely to have a better understanding of its material properties and facilitate the numerical study of the effect of fiber-reinforced polymers in composite rebar. The #3 rebar sample has a length of 8 in, is equipped with a strain gauge at the midspan to measure the tensile strain. The experiment is conducted using an INSTRON universal testing machine, which has a maximum load capacity of 50 kN.

From the tensile test results, the composite reinforcement exhibits linear material property, consistent with the rebar product specifications.
We also test the compressive strength of concrete samples to use as input for finite element analysis (FEA), following the ASTM C39/C39M-21 standard. Three 4 in × 8 in cylindrical specimens are prepared and tested for their 8-day compressive strength, aligning with the curing age of 8 days for three-point flexural testing of smart composite reinforced beams. The applied loading rate during the tests was 0.27 MPa/s. Figure 6(a) illustrates a cylindrical concrete sample positions in a Forney automatic compression test machine. The pad cap system used in the tests consists of reusable pads housed within steel retainer rings, ensuring uniform load distribution on the ends of the concrete cylinders during compression testing. Figure 6(b) shows a fractured cylindrical concrete sample after compression. The measured compressive strengths of the samples are 35.52 MPa, 35.73 MPa, and 36.06 MPa, respectively. The variance among the results was 0.8%, which is within the acceptable range, confirming the reliability of the experimental data. Based on the test results, the average compressive strength of 35.77 MPa is selected for use in numerical studies.

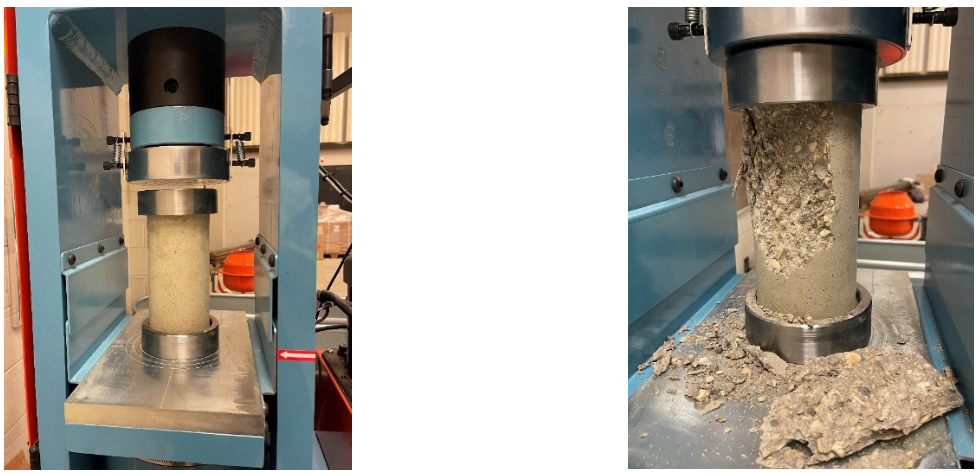

(a) (b)

Figure 6. (a) The cylindrical concrete sample ready for test. (b) The fractured cylindrical concrete sample after compression.

Overall, in Task 1, we successfully develop smart composite reinforcement in concrete beams and demonstrate the real-time monitoring of composite reinforcement. The results from two types of smart sensors align well with each other. And the strain data is validated by images and videos, recorded by different types of cameras, showing the accuracy and reliability of our smart sensor-based testbed. The experiment results are integrated with the numerical results from Task 2, and used as input to train machine learning algorithms in Task 3.

2.2 Task 2: Multi-scale multi-physics modeling with finite element analysis for the composite reinforcement mechanical and bonding performance

In this task, we conduct three-dimensional (3D) finite element analysis (FEA) to simulate mechanical and bonding performance of composite reinforced concrete. The numerical modeling results in this task are used as complementary of the experimental and sensor data in Task 1 to establish a physics-informed database for machine learning algorithms in Task 2. After numerically validate the accuracy of our FEA with experimental results, we simulate the flexural test and pull-out test of the reinforcement-concrete system by considering various factors such as types of composite rebars, strength of concrete materials, and rebar configurations. We apply Abaqus for the numerical modeling of both flexural strength test and pull-out test.

2.2.1 Numerical Validation

In this task, we computationally investigate the mechanical behaviors of smart composite reinforced concrete and validate our numerical models with sensor data in Task 1. To enhance computational efficiency, a quarter finite element model (FEM) is constructed in ABAQUS software, representing the experimental setup symmetrically. This approach reduces computational demand while maintaining the integrity of the analysis. All other configurations, including material properties, boundary conditions, and loading rate, are kept identical to those in the laboratory experiment to ensure consistency between experimental and numerical studies. For material property simulation, the concrete damage plasticity (CDP) model is employed for concrete, and the elasto-plasticity model is used for the composite reinforcement in nonlinear static analysis. Based on the compressive strength of concrete, which is tested to be 35.77 MPa, the elastic Young's modulus is calculated as 30,010.2 MPa using ACI 318-19 specifications, and the Poisson’s ratio is set to 0.2. The plasticity behavior of concrete is defined using the following parameters: a dilation angle of 30°, eccentricity of 0.1, a biaxial-to-uniaxial compressive strength ratio of 1.16, a tensile meridian ratio of 0.66, and a viscosity parameter of 0.001 [3]. Concrete compression and tensile behavior, as well as associated damage parameters, are calculated based on [4].

For the numerical validation, the strain data in the composite reinforcement FEA are critical. To ensure accuracy, the mesh around the circumferential direction is refined to capture more precise results. Figures 7 shows the strain comparison between the distributed fiber optic sensor (DFOS), strain gauge, and FEA results. It should be noted that the noise in sensors make them difficult to directly compare with FEA results. A butterworth filter is employed to denoise the sensor data. Due to the significant different sampling rates of two sensors, customized filters are designed and applied to process their data separately. A notable observation is that the strain spike in FEA appears approximately 30 seconds earlier than the sensors capture it, suggesting that the initial flexural crack is detected earlier in the numerical model compared to the experiment. Despite this timing discrepancy, the FEA results show high overall agreement with the DFOS and strain gauge data before the flexural crack initiates in FEA and after the experimental flexural crack occurrence. This validation underscores the reliability of the FEA model in simulating the mechanical behavior of the composite reinforcement under flexural load.

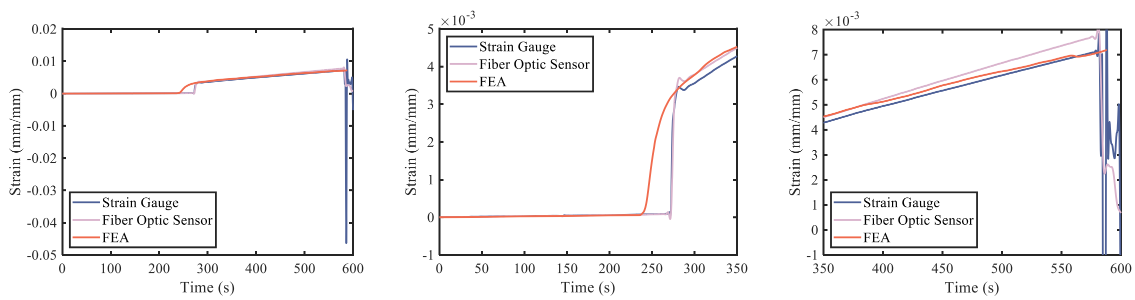

(a) (b) (c)

Figure 7. Longitudinal strain at the midspan of reinforcement. (A) Whole phase – 600s, (b) First phase - 0 - 350 s, and (c) Second phase – 350 - 600s.

Additionally, the distributed strain measurement capability of DFOS allows for real-time monitoring of longitudinal strain along the composite reinforcement. To further validate the numerical model, the strain distribution along the reinforcement is compared with FEA results at six time slots, as illustrated in Figure 8. During the uncracked state of the concrete, the strain in the composite reinforcement can be estimated theoretically [5]. Figure 8(a) and (b), which represent strain along the reinforcement at 100 seconds and 200 seconds, demonstrate that the numerical results are well-aligned with the DFOS experimental data and theoretical predictions. Once the flexural crack initiates, the theoretical method becomes inapplicable. Across all these time slots, the numerical results exhibit excellent agreement with the experimental data, further validating the accuracy and reliability of the FEA model in simulating composite reinforced concrete structure under varying conditions.

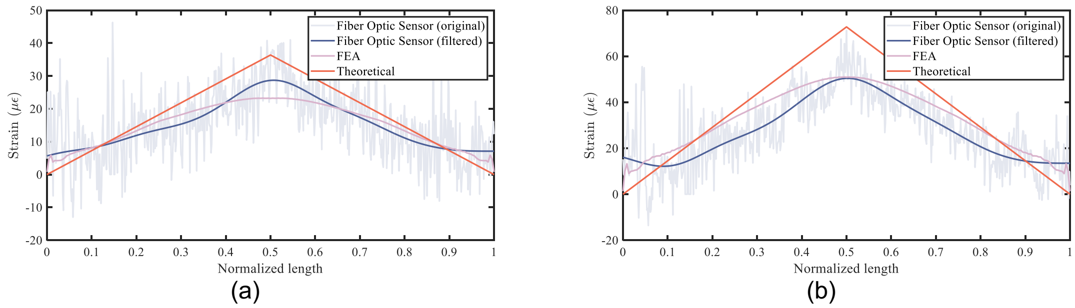

Figure 8. The longitudinal strains on composite reinforcement. (a) 100s; (b) 200s.

<u>2.2.2 Flexural Test Analysis</u>

After validating numerical models, the FEA models are used to establish a comprehensive physics-informed database together with experimental results by considering different scenarios and factors in composite reinforced concrete systems. The database is utilized to train machine learning-based condition assessment algorithms in Task 3. In this task, we consider four concrete grades, including normal concrete with a compressive strength of 5,000 psi, concrete aligned with the experimental value of 5,188 psi (35.77 MPa), high-performance concrete (HPC) with a compressive strength of 10,000 psi, and ultra-high-performance concrete (UHPC) with a compressive strength of 22,000 psi. In addition to concrete grades, we also broaden the selection of composite rebar materials. We simulate four types of most widely used FRPs in the composite rebars: aramid FRP (AFRP), basalt FRP (BFRP), carbon FRP (CFRP), and glass FRP (GFRP) in our study. All simulated composite rebars have a uniform diameter of 3/8 inches and a length of 18 inches. Furthermore, we investigate the effect of rebar ribs on the performance of composite reinforced concrete systems. The bond strength of ribbed GFRP rebar is primarily influenced by the mechanical interaction between the ribs and the surrounding concrete. As a result, the bond-slip behavior of GFRP ribbed rebars can vary depending on the geometries of the ribs [6]. The geometries of the composite rebars are established according to the reference [7]. Figure 9 provides detailed schematics of the specific geometries for AFRP, BFRP, CFRP, and GFRP rebars, along with FRPs without ribs.

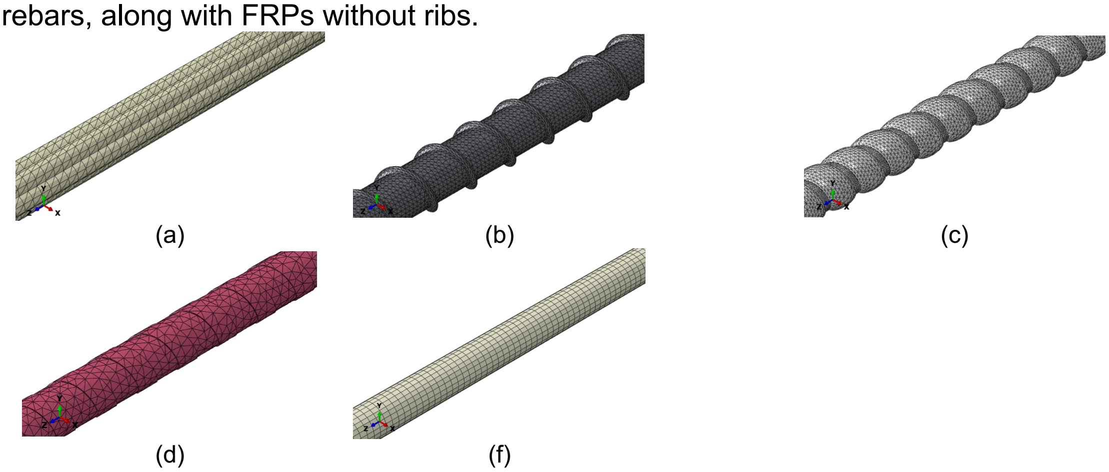

Figure 9. Simulation details for different types of FRP: (a) AFRP, (b) BFRP, (c) CFRP, (d) GFRP, and (f) No ribs rebar.

We model 36 cases evaluating the effects of concrete strength, rebar geometry, FRP material properties, and bonding conditions (embedded and cohesive) among four different types of FRP rebars: AFRP, BFRP, CFRP, and GFRP. The concrete strength ranges from 5,000 psi to 22,000 psi. This combination model is designed to predict how variations in these parameters influence the structural performance of composite reinforced concrete systems, offering a comprehensive understanding of their mechanical behavior. The comparison of different contact interaction models reveals distinct outcomes in simulating the rebar strain distribution and concrete crack behavior in composite reinforced concrete systems. Figure 10(b)-(e) illustrate that FEA prediction of the concrete damage pattern aligns closely with experimental crack propagation shown in Figure 10(a).

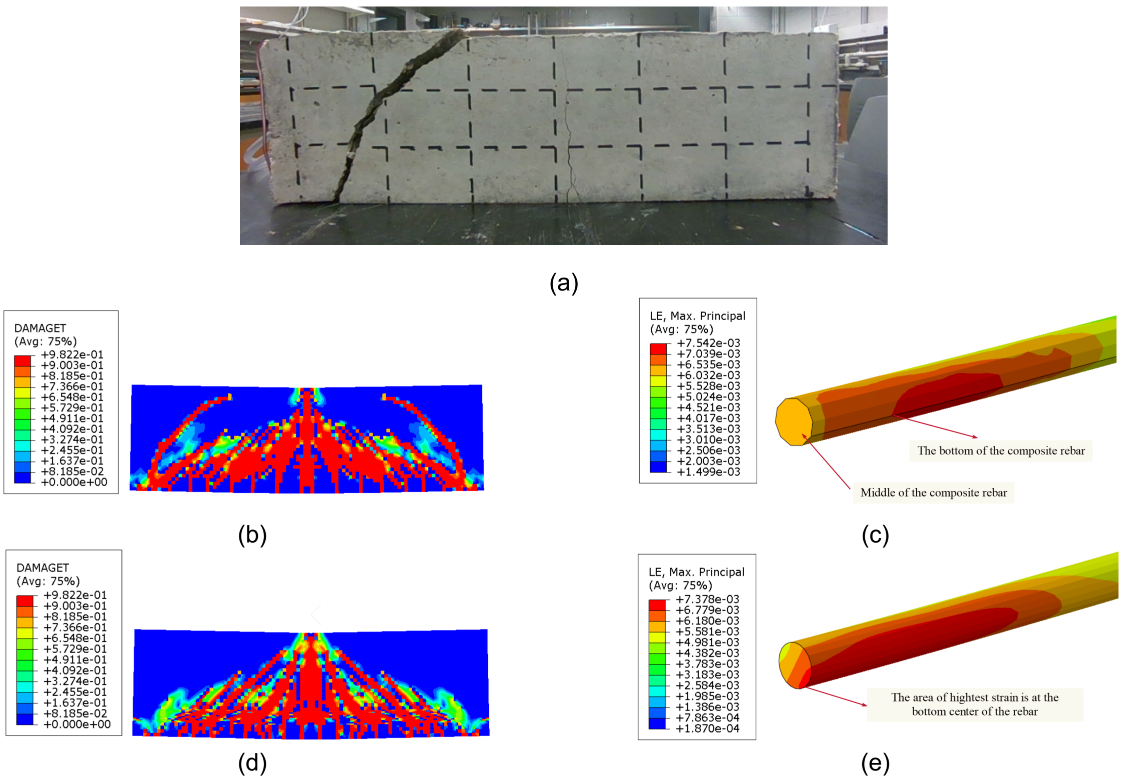

Figure 10. Comparison of numerical simulation results for composite reinforced concrete systems. (a) experimental crack propagation; (b) DAMAGET using embedded contact interactions; (c) Rebar strain distribution using embedded contact; (d) DAMAGET using cohesive behavior; (f) Rebar strain distribution using cohesive behavior.

2.2.3 Pullout Test Analysis

In this section, we focus on the numerical modeling of the bonding performance of composite reinforced concrete through the simulation of a pull-out test. For the pull-out test of the reinforcement-concrete system, simulations are conducted using SIMULIA-ABAQUS [8]. The pull-out simulation is conducted based on the specified composite rebar bonding strength test standard ASTM-D7913M [9]. We apply the same GFRP rebars as previous section with the material properties: Young's modulus of 46.88 GPa, Poisson's ratio of 0.3, and ultimate strength of 1,003 MPa. The plasticity parameters for the CDP model are specified as follows: a dilation angle of 30 degrees, eccentricity of 0.1, a ratio of biaxial compressive strength to uniaxial compressive strength of 1.16, and a ratio of the second stress invariant on the tensile meridian of 0.66 [3]. Accurately representing rib geometry is essential, as optimal rib geometries can enhance bond performance [10]. The rib geometry is based on the actual measurements of the physical PINKBAR rebars. We calibrate our FEA model for the pull-out test by comparing the crack pattern using DAMAGET and bonding stress-displacement curve with the reference. As shown in Figure 11(a), the FEA model exhibits splitting cracks, which is aligned with the experimental results reported by Metelli & Plizzari [11]. Figure 11(b) shows a comparison of bonding stress-displacement curve from our FEA and results from Seok et al. [12].

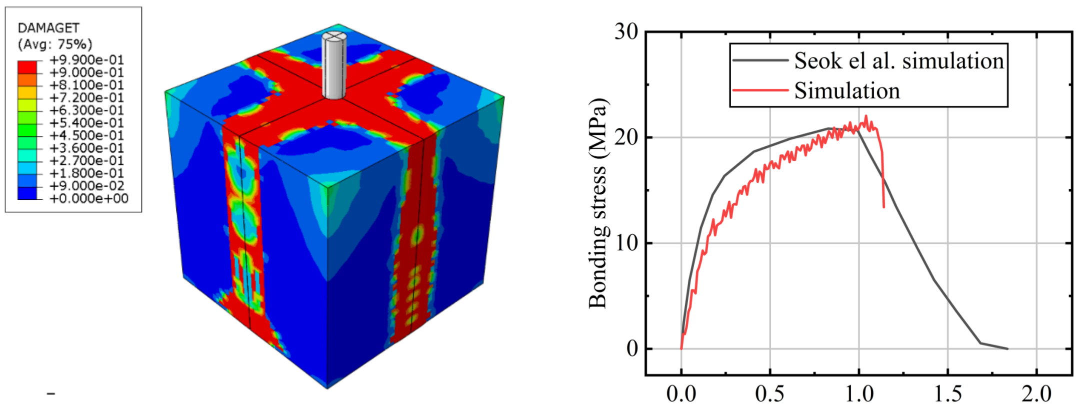

(a) (b)

Figure 11. Pull-out simulation results: (a) external cracking pattern; (b) comparison of bonding stress results.

2.3 Task 3: AI-Driven condition assessment for composite reinforced concrete

In this task, our main research objective is to develop a condition assessment framework for composite reinforced concrete. Sufficient data from FEA simulations and experiments from Tasks 1 and 2 are employed to train machine learning and neural network models. We use two methods for condition assessment: the DAMAGET and the crack size.

<u>2.3.1 Condition Assessment using DAMAGET Data</u>

In this section, we train the machine learning (ML)-based condition assessment algorithms using the finite element results of the three-point flexural test. We define the condition based on the crack propagation data during the flexural test. DAMAGET stands for "Tensile Damage Initiation" which is used to describe a level at which a material starts to be damaged in tension [15]. Specifically, when the tensile stress of the material reaches the threshold defined by DAMAGET, Abaqus starts to calculate the damage variables and simulate the damage behavior of the material. Higher DAMAGET values indicate greater tensile damage in the elements. In this way, DAMAGET could be a metric for the condition prediction of composite beams. Thus, we train the DAMAGET data at different time steps generated from the FEA results in Task 2.

For the three-point flexural test, the DAMAGET values at the surface of the beam across varying loading conditions are compiled into a dataset to train the machine learning model. We applied seven machine learning algorithms to train (80%) and test (20%) the FEA dataset. Figure 12. compare the performance of each ML algorithms.

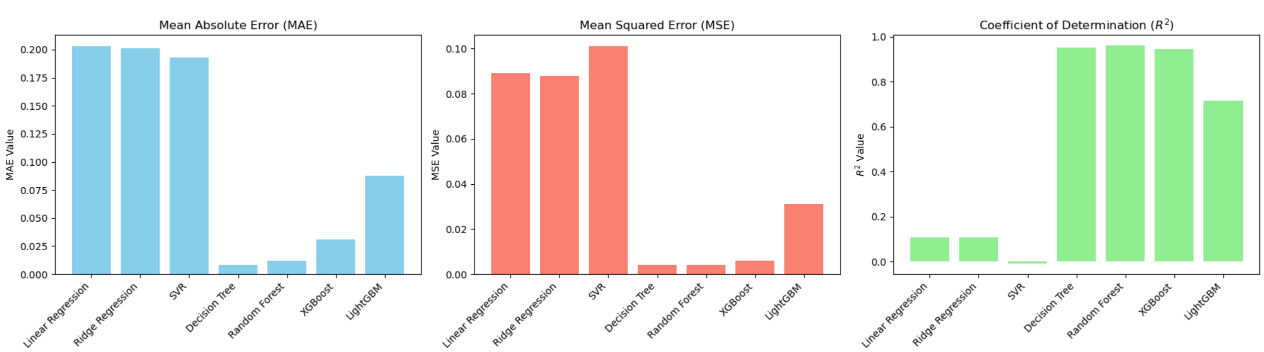

Figure 12. Performance of different machine learning algorithms in condition assessment from DAMAGET data

As shown in Figure 12, linear algorithms, for example, Ridge Regression, have poor performance in DAMAGET predictions. However, tree-like algorithms show a better effect, their goodness of fit is almost all above 0.9. Therefore, we choose random forest regression algorithm for condition assessment from DAMAGET data. Figure 13 shows the ML prediction results on crack patterns of the composite reinforced concrete system by comparing the DAMAGET distribution at t = 0.6 s (or displacement = 3 mm) predicted by FEA and random forest regression algorithm. The condition index is obtained by normalizing the value of DAMAGET into 0 to 1. According to the comparison result, random forest regression provides a prediction with R^2 = 0.96, MSE = 0.004, and MAE = 0.012. To some extent, R^2 can be considered as the proportion of accuracy predicted by regression. R^2 = 0.96 indicates the accuracy of the prediction.

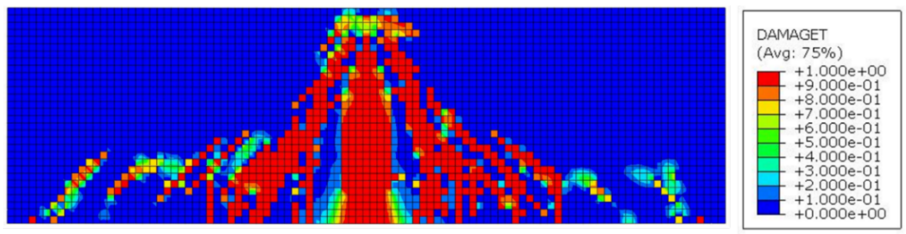

(a)

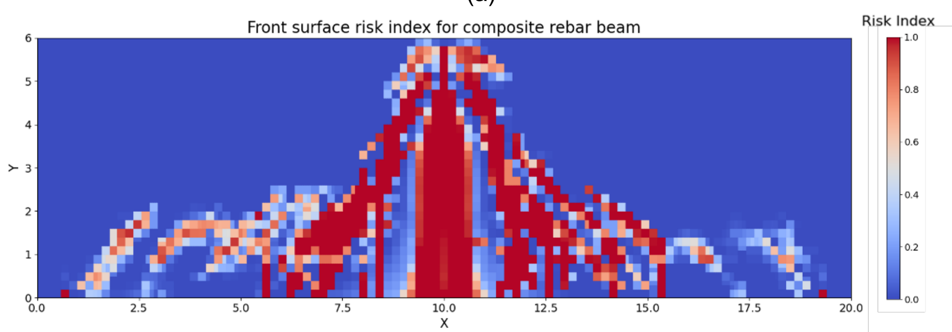

(b)

Figure 13. Comparison between FEA (a) and ML (b) results at t=0.6s.

Similarly, we train machine learning-based condition assessment models using DAMAGET from FEA of the pull-out test. For the pull-out test, the DAMAGET values at different surfaces are compiled into a dataset to train the condition model. We applied five machine learning algorithms to train (80%) and test (20%) the FEA dataset of the bottom surface. Similar to the training from FEA of flexural test, random forest regression algorithm has the best performance on condition prediction since it has the highest R^2 and lowest MSE and MAE. After the random forest model is fully trained, it can be used to predict the condition index at different time steps. To illustrate crack propagation from the inner surface to the outer surface, we analyze a quarter of the pull-out model. The condition index is obtained by normalizing the value of DAMAGET into 0 to 1. To some extent, R^2 can be considered as the proportion of accuracy predicted by regression. The lowest R^2 still reaches 0.89, indicating the prediction is accurate. Figure 14 shows comparisons between the DAMAGET distribution from FEA and condition distribution from ML at the final time step.

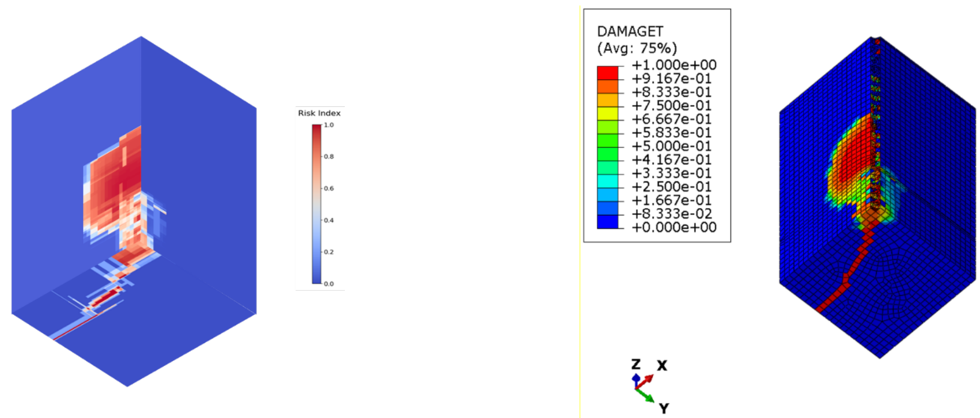

(a) (b)

Figure 14. Comparison between FEA simulation and ML prediction in 3D views of the pull-out test results: (a) machine learning prediction; (b) FEA simulation.

2.3.2 Condition Assessment using Image Data

In this task, we develop a rapid prediction method was proposed in the research which is based on convolutional neural network (CNN). The DAMAGET images obtained from FEM simulation is RGB format which means they are colorful. However, most of time, the actual crack images collected from the experiments are in gray and treated as binary images. Hence, we also test the performance of the model by training with binary DAMAGET images. Comparing with the FEM simulation, the CNN method only needs 0.61 second by using Intel® Core™ i7-10700 processor, which demonstrate a great potential for practical applications. We obtain the simulation and experiment results of smart composite reinforcement-concrete system. In this task, we develop a rapid prediction method was proposed in the research which is based on convolutional neural network (CNN). Figure 15 shows the basic steps of the proposed method. At this stage, we utilized the DAMAGET images as the input, and the output is the maximum strain of the rebar, which are collected from our FEA model. The DAMAGET images have same patten as the cracks in the experiment.

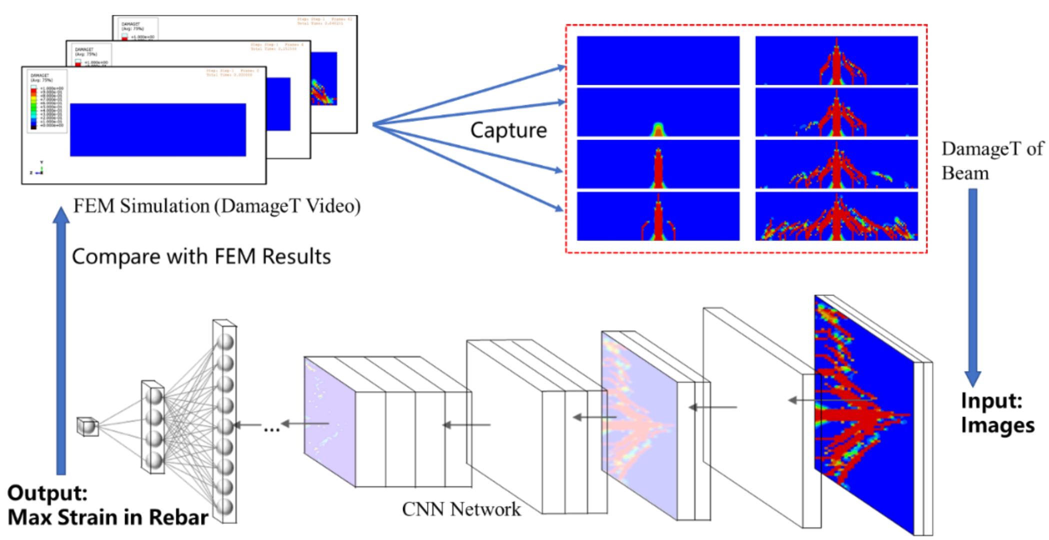

Figure 15. Schematic of strain Prediction by CNN.

Comparing with regression which uses all the data for training, prediction tasks divide data sets into training and test parts which are strictly disjoint. Hence, using this method, the model we obtain can demonstrate the ability to perform calculations by using unknown data (Generalization

Ability). In the study, we use 70% of data for model training and 30% data for performance test. Hence, the model we trained would be more practical and stronger. In this task, we adopt ResNet34 as the basic model because of its flexibility on large number of parameters and the special residual structure to better extract features from images. An essential requirement of prediction tasks is sufficient amount of data. Therefore, in the research, we generate a more precise FEA model which has a smaller time step. The amount of data used in the study expand tenfold, from 64 to 640 data points. We transform the colorful DANAGET images into binary images, shown in Figure 16.

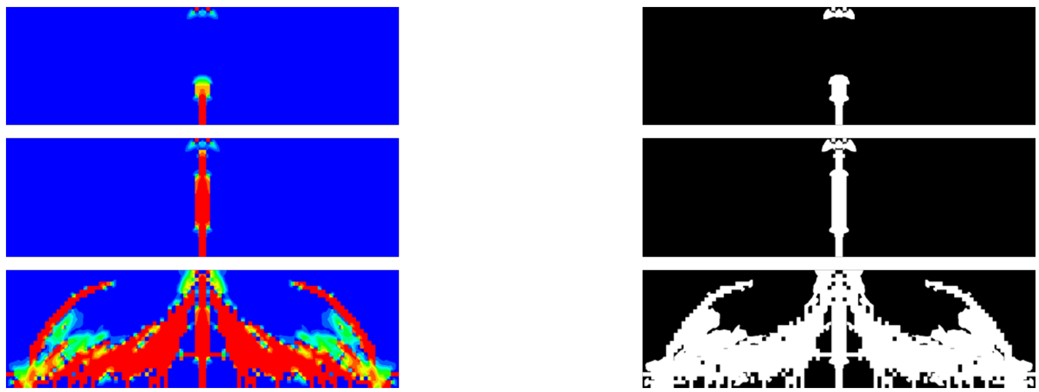

Figure 16. Colorful DAMAGET and binary DAMAGT.

After training, the rest 30% dataset is used to demonstrate the ability of model prediction. We also use the same setting to train a LeNet5 as a comparison. The prediction performance of ResNet34 and LeNet5 is shown in Figure 17. The R^2 values of ResNet34 and LeNet5 are 0.99 and 0.90. ResNet34 shows superior performance in the conduction assessment from image data.

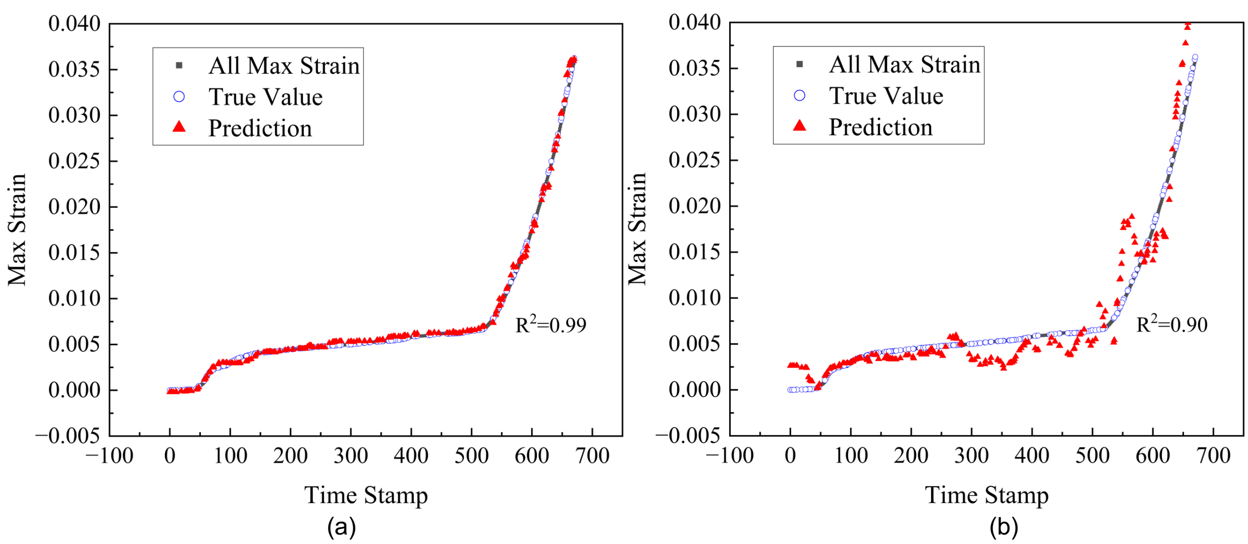

Figure 17. (a) prediction results of ResNet34; (b) prediction results of LeNet5.

3. Educational outreach activities

The PIs organized their research teams for the composite reinforced concrete beam testing day on September 13, 2024, shown in Figure 18.

Figure 18. Concrete beam test day, Sep 13, 2024.

In addition, as shown in Figure 19, the PI and her graduate and undergraduate students have recently filmed a series of K-12 educational videos about sustainable construction materials and resilient infrastructure posted on YouTube as part of Purdue's Superheroes of Science Series.

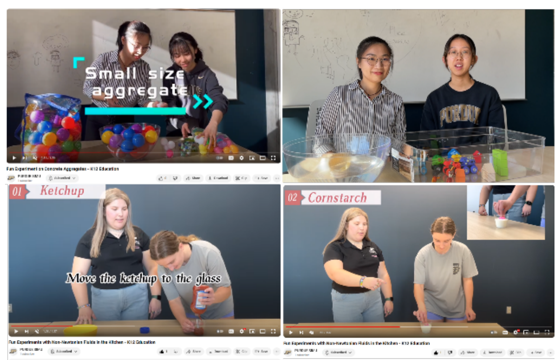

Figure 19. K-12 education videos filmed by PI's group

4. Workforce development activities
N/A

5. Technology transfer actions
N/A

6. Papers that include TRANS-IPIC UTC in the acknowledgments section
Our team submitted one journal paper "*Computational Investigation and Spatial-Temporal Risk Assessment of Reinforced Concrete Failure with Metallic and Composite Reinforcements Transportation Research Board*" to Buildings and is still under review.

7. Presentations and posters of TRANS-IPIC funded research

- Tao, C., & Junyi Duan, "Data-driven smart composite reinforcement for precast concrete", TRANS-IPIC Monthly Research Webinar, September 23, 2024.
- Tao, C., Guan, S, Duan, J., Lin, Y., & Yan, H. (2024). Data-Driven Smart Composite Reinforcement for Precast Concrete, U.S. Department of Transportation (USDOT) - University Transportation Center (UTC), Transportation Infrastructure Precast Innovation Center (TRANS-IPIC) Workshop, Chicago, IL, April 22, 2024.

8. Any other events or activities that highlights the work of TRANS-IPIC research that occurred at your university

N/A

9. Any mentions/references to TRANS-IPIC in the news or interviews from your research

- Purdue Polytechnic News:
https://polytechnic.purdue.edu/newsroom/polytechnic-research-awards-february-2024
- Twitter of Purdue Institute for a Sustainable Future, shown in Figure 20.

Figure 20. News on the twitter of Purdue Institute for a Sustainable Future

10. References associated with this research project

[1] E. Hamed, 'Load-carrying capacity of composite precast concrete sandwich panels with diagonal fiber-reinforced-polymer bar connectors', *PCI J*, vol. 62, no. 4, pp. 34–44, 2017.

[2] M. F. Bado et al., 'Distributed optical fiber sensing bonding techniques performance for embedment inside reinforced concrete structures', *Sensors*, vol. 20, no. 20, p. 5788, 2020.

[3] S. Seok et al., 'Finite element simulation of bond-zone behavior of pullout test of reinforcement embedded in concrete using concrete damage-plasticity model 2 (CDPM2)', *Engineering Structures*, vol. 221, p. 110984, 2020.

[4] L. Qingfu et al., 'Parameter calculation and verification of concrete plastic damage model of ABAQUS', in *IOP conference series: Materials science and engineering*, 2020, vol. 794, no. 1, p. 012036[Online]. Availablehttps://iopscience.iop.org/article/10.1088/1757-899X/794/1/012036/meta[Accessed: 23November2024].

[5] C. G. Berrocal et al., 'Crack monitoring in reinforced concrete beams by distributed optical fiber sensors', *Structure and Infrastructure Engineering*, vol. 17, no. 1, pp. 124–139, Jan. 2021 [Online]. Available: 10.1080/15732479.2020.1731558.

[6] Q. Hao et al., ‘Bond strength improvement of GFRP rebars with different rib geometries’, *J. Zhejiang Univ. - Sci. A*, vol. 8, no. 9, pp. 1356–1365, Aug. 2007 [Online]. Available: 10.1631/jzus.2007.A1356.
[7] K. Brózda et al., ‘ANALYSIS OF PROPERTIES OF THE FRP REBAR TO CONCRETE STRUCTURES’, vol. 2, no. 1, 2017.
[8] ‘Dassault Systèmes. (Year). Abaqus/CAE User’s Manual. Retrieved from [Abaqus/CAE User’s Manual (6.12)]’. .
[9] ‘ASTM D7913M Standard Test Method for Bond Strength of Fiber-Reinforced Polymer Matrix Composite Bars to Concrete by Pullout Testing’. .
[10] Q. Hao et al., ‘Bond strength of glass fiber reinforced polymer ribbed rebars in normal strength concrete’, *Construction and Building Materials*, vol. 23, no. 2, pp. 865–871, Feb. 2009 [Online]. Available: 10.1016/j.conbuildmat.2008.04.011.
[11] G. Metelli and G. A. Plizzari, ‘Influence of the relative rib area on bond behaviour’, *Magazine of Concrete Research*, vol. 66, no. 6, pp. 277–294, Mar. 2014 [Online]. Available: 10.1680/macr.13.00198.
[12] S. Seok et al., ‘Finite element simulation of bond-zone behavior of pullout test of reinforcement embedded in concrete using concrete damage-plasticity model 2 (CDPM2)’, *Engineering Structures*, vol. 221, p. 110984, Oct. 2020 [Online]. Available: 10.1016/j.engstruct.2020.110984.
[13] A. Hu et al., ‘Bond Characteristics between High-Strength Bars and Ultrahigh-Performance Concrete’, *J. Mater. Civ. Eng.*, vol. 32, no. 1, p. 04019323, Jan. 2020 [Online]. Available: 10.1061/(ASCE)MT.1943-5533.0002919.
[14] A. A. Soliman et al., ‘Effects of the tensile properties of UHPC on the bond behavior’, *Construction and Building Materials*, vol. 392, p. 131990, Aug. 2023 [Online]. Available: 10.1016/j.conbuildmat.2023.131990.
[15] I. Drygala et al., ‘Numerical evaluation of seismic-induced damages in masonry elements of historical arch viaduct’, in *IOP Conference Series: Materials Science and Engineering*, 2018, vol. 364, no. 1, p. 012006[Online]. Availablehttps://iopscience.iop.org/article/10.1088/1757-899X/364/1/012006/meta[Accessed: 29June2024].
[16] 318 ACI Committee, *Building code requirements for structural concrete (ACI 318-08) and commentary*. American Concrete Institute, 2008[Online]. Availablehttps://books.google.com/books?hl=zh-CN&lr=&id=c6yQszMV2-EC&oi=fnd&pg=PT10&dq=Building+Code+Requirements+for+Structural+Concrete+(ACI+318-08)+and+Commentary&ots=nZNrMX4yPF&sig=5FmtjAhkD_oWZdKzVcapZ34cqME[Accessed: 27September2024].
[17] R. M. Haralick, ‘Using perspective transformations in scene analysis’, *Computer Graphics and Image Processing*, vol. 13, no. 3, pp. 191–221, Jul. 1980 [Online]. Available: 10.1016/0146-664X(80)90046-5.
[18] Y. LeCun et al., ‘Gradient-based learning applied to document recognition’, *Proceedings of the IEEE*, vol. 86, no. 11, pp. 2278–2324, 1998.